Article

S Band Hybrid Power Amplifier in GaN Technology with Input/Output Multi Harmonic Tuned Terminations

Sandro Ghisotti [1] , Stefano Pisa[1] and Paolo Colantonio [2]

[1] Department of Information Engineering Electronics and Telecommunications, Sapienza University of Rome, Italy, sandro.ghisotti@uniroma1.it, stefano.pisa@uniroma1.it
[2] University of Roma Tor Vergata, Electronic Engineering Department, Via del Politecnico 1, 00133 Roma, Italy; paolo.colantonio@uniroma2.it
* Correspondence: sandro.ghisotti@uniroma1.it

Abstract: In this paper, the design, fabrication, and measurements of an S band multi harmonic tuned power amplifier in GaN technology is described. The amplifier has been designed by exploiting second and third harmonic tuning conditions at both input and output ports of the active device. The amplifier has been realized in a hybrid form and characterized in terms of small and large signal performance. An operating bandwidth of 300 MHz around 3.55 GHz, with 42.3 dBm output power, 9.3 dB power gain and 53.5 % of power added efficiency PAE (60 % drain efficiency) at 3.7 GHz are measured.

Keywords: power amplifier (PA); gallium nitride (GaN); harmonic terminations (HT); power added efficiency (PAE)

Citation: Ghisotti, S.; Pisa, S.; Colantonio, P. S Band Hybrid Power Amplifier in GaN Technology with Input/Output Multi Harmonic Tuned Terminations. *Electronics* **2021**, *1*, 0. https://doi.org/

Received:
Accepted:
Published:

Publisher's Note: MDPI stays neutral with regard to jurisdictional claims in published maps and institutional affiliations.

Copyright: © 2021 by the authors. Submitted to *Electronics* for possible open access publication under the terms and conditions of the Creative Commons Attribution (CC BY) license (https://creativecommons.org/licenses/by/ 4.0/).

1. Introduction

The great innovations in the wireless communication systems, such as cellular phones, satellite payloads and microwave transponders, just to name a few, have led power amplifiers (PAs) to become a crucial device to properly amplify modulated signals employed in such systems [1].

High linearity, output power and efficiency (power added efficiency, PAE), represent the main features of a PA, which are conflicting with each other, thus demanding some design trade off.

Moreover, being the PA the most power-consuming sub-system in a transmitting chain, the goal of reaching the highest efficiency value becomes a discriminating factor for the successful development of wireless systems, simplifying the structure of the cooling system as well [2]. As far as efficiency improvement is concerned, the bias point can be shifted from class A toward class AB, thus reducing the conductive angle while sacrificing the gain [3]. For narrow-band applications (roughly up to 10% of fractional bandwidth), the waveform engineering technique, i.e., the shaping of the voltage and current wave-forms at the active device output, improves the attainable efficiency by simultaneously lowering the dissipated power (waste) in the active device, while increasing its output power delivered to the load at fundamental frequency.

Going into some detail on that, several harmonic terminating design strategies have been developed and proposed. In this regard, the tuned load configuration tries to reach a sinusoidal output voltage waveform by loading with a short circuit the second and third output voltage harmonics [3]. Class F amplifiers aim to achieve a rectangular output voltage waveform by loading the third output harmonic with an open circuit, shortening the second ones. In the process, the main PA features are going to be improved with respect to the tuned load configuration [4–6]. More in general, in harmonic tuned power amplifiers (HTPAs) the generation and control of second and third harmonic terminations, both at the input and output device ports, are performed [7–10]. The final outcomes have shown performance improvements in terms of efficiency, output power and power gain, with respect to the tuned load and class F cases [3]. On the other hand, HTPA designers have to deal with a major complexity design in order to generate output harmonic components with the proper phase relationships.

To improve the PA efficiency, other approaches based on device switching mode operation have been proposed, such as Class D (or S) [11,12] and Class E [13], which demonstrated to be effective for low operating frequencies (less than a few GHz).

As far as PA frequencies are concerned, 5G technology standard for cellular network foresees two different frequency ranges, namely the sub-6 GHz region (FR1) and the mm wave frequencies (FR2), where the FR2 networks are expected to provide very high data rates across small network cells (pico cells) [14]. The first 5G networks will employ sub-6 GHz frequencies and have comprised large cells in cities and rural areas. They will transmit high-power RF signals (>10W) over large areas, or "macro cells", each requiring a high-efficiency linear power amplifier to avoid unnecessary power consumption during transmission [14,15]. One of the sub-6 GHz bands for Europe lies in the S band, between 3.4 GHz and 3.8 GHz [16].

In this paper, the design, realization and test of a hybrid S-band PA, biased in deep class AB over a frequency range from 3.4 GHz to 3.7 GHz, is presented. The harmonic tuning approach based on input and output multi harmonic manipulation is used.

This paper is organized as follow: in Section 2, a brief overview on the basic of harmonic manipulation is recalled, while in Section 3 the PA design and its practical realization are presented. Performance features achieved from experimental measurements in terms of scattering parameters (small signal conditions) and output power, power gain and PAE (large signal conditions) are discussed in Section 4.

The designed class AB-HTPA achieves a PAE higher than 55 % and an output power greater than 41 dBm over a frequency range from 3.4 GHz to 3.7 GHz in simulation. In measurement, it achieved a PAE of 53.5 % (efficiency 60 %) and an output power of 42.3 dBm at the frequency f_0 = 3.7 GHz, in line with simulation expectations. An output power larger than 40 dBm with a PAE greater than 40 % was measured in a frequency range from 3.5 GHz to 3.9 GHz.

2. Harmonic Manipulation Basic

Power amplifiers are inherently based on the use of nonlinear active devices, whose output (and input) loading harmonic impedances are suitable optimized to shape its output voltage waveform, while preserving the shape of the output current waveform, regardless the device physical nature (e.g., HBT, HEMT, etc.). In a generic class B, the device is turned off for half the period of the RF excitation signal, and its output current is usually approximated as a half sinusoid, whose harmonics are terminated across the output matching network. Similarly, other non-linear mechanisms can create current harmonic components, e.g. deviations from the class B bias point and the nonlinear device capacitances and transconductance. In generic Field Effect Transistors, the nonlinear gate-source (C_{gs}) and gate-drain C_{gd}) capacitances may directly create harmonic components at the gate of the active device as well [17]. Moreover, at higher frequencies the feedback mechanisms generated by C_{gd} can couple drain harmonics to the gate. Thus, the gate voltage waveform can no longer be considered as a pure sine wave and, as a result, the drain current deviates from an ideal half sinusoidal shape.

From a practical standpoint, harmonic termination impedances in an HTPA must be exploited to properly shape both the gate voltage and drain current waveforms [18].

Assuming the active device (in the following considered as FET type) acting as a voltage controlled current source, the drain current waveform is shaped by the input voltage, whereas the output voltage waveform is controlled and shaped by the output load impedances [19].

In terms of current and voltage harmonic components $I_d(nf_0)$ and $V_{ds}(nf_0)$, respectively, the above statement may be written as:

$$i_D(t) = I_{DD} + \Re e \left\{ \sum_{n=1}^{\infty} I_d(nf_0) e^{j2\pi \cdot n \cdot f_0 \cdot t} \right\} \tag{1}$$

$$V_{ds}(nf_0) = Z(nf_0) \cdot I_d(nf_0) \tag{2}$$

$$v_{DS}(t) = V_{DD} - \Re e \left\{ \sum_{n=1}^{\infty} V_{DS}(nf_0) e^{j2\pi \cdot n \cdot f_0 \cdot t} \right\} \tag{3}$$

where $Z(nf_0)$ is the impedance seen by the drain current generator at the n-th harmonic frequency, V_{DD} and I_{DD} are the bias voltage and current (quiescent), respectively. Equation (2) describes two different ways of shaping the waveform of $V_{ds}(nf_0)$, namely by $I_d(nf_0)$ (operating an appropriate input harmonic matching network), or by $Z(nf_0)$ (operating an appropriate choice of the output matching network). The frequency components controlled in an actual design are typically limited up to the third harmonics (n = 1, 2, 3), just to reduce the circuit complexity and the inherent increases in the losses that would nullify the benefits linked to a control of the upper harmonics. Moreover, for high frequencies applications, the higher order components may usually be considered practically shorted by the capacitive behavior of the transistor at its input and output ports. Hence, a general scheme of the harmonic control technique is represented in Fig. 1.

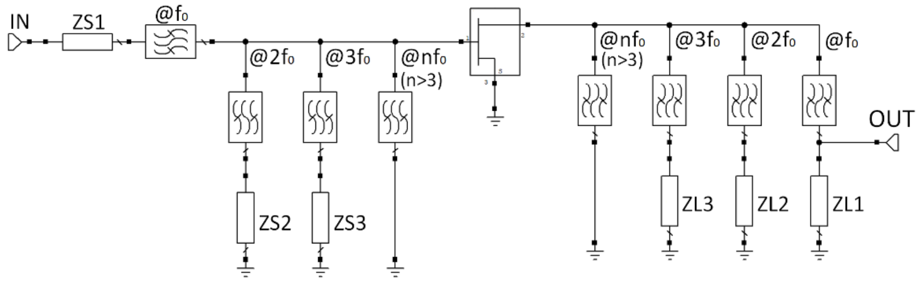

Figure 1. Matching networks of an HT PA.

In the reported scheme, the input matching network (ZS1 and filter @f_0) has to assure at the fundamental frequency the conjugate matching criterion over the operating bandwidth. At the same time, exploiting the non-linear behavior of the active device at its input, the appropriate choice of the input harmonic terminations (ZL2, @$2f_0$; ZL3, @$3f_0$) allows to shape the v_{GS} voltage waveform (i.e., the FET input controlling signal), which ultimately controls the generation of the output drain current harmonic components $I_d(nf_0)$.

As far as output is concerned, the maximum output power delivered by the active device is attained by simultaneously maximizing its voltage and current swings.

Because current and voltage at the fundamental frequency must be in phase at the intrinsic terminal of the active device nonlinear current source, the role of the output matching network (ZL1, @f_0) is to achieve a purely resistive loading of the controlled source [20]. On the other hand, the other output matching networks (ZL2, @$2f_0$; ZL3, @$3f_0$) are used to properly shape the device output voltage waveforms v_{DS}, according to equation (3).

Summing up what has been stated so far, the goal of the multi harmonic manipulation procedure is to achieve an increase in fundamental frequency voltage component with respect to the case where no harmonic components are present (tuned load configuration). Therefore, a higher output power and efficiency values are achieved.

In this work, the harmonic tuning methodology based on the control of the fundamental, second and third harmonic components, at the input and output ports of the active device, has been adopted. The control will be carried out by the proper passive termination at each harmonic component. Harmonic components order higher than 3 have been assumed shorted by the device output capacitive effect.

3. Power Amplifier Design

3.1. Active Device Technology

The Gallium Nitride (GaN) technology shows attractive features due to its high breakdown voltage, high temperature stability, and high power density [21,22]. Moreover, the swing of a GaN device output voltage is mostly limited by its ohmic region rather than its gate–drain breakdown. From this standpoint, HT design strategy may be an attractive choice for a GaN power amplifier.

In this work, the active device CREE CG2H40010, a packaged 10 W GaN HEMT, has been selected. A non-linear device model, provided by the manufacturer, has been employed in the AWR Microwave Office design software.

The microwave substrate used for the design is 10mil Rogers RT/duroid 6010.2LM microwave laminates, chosen for its high constant dielectric of 10.7, which makes the size of the final circuit smaller.

3.2. Bandwidth, Biasing and Stability Network

For the design of the power stage, the center frequency f_0 = 3.55 GHz with 300 MHz of bandwidth (8.4 % of fractional bandwidth) has been adopted, while a class-AB bias condition with V_{DS} = 28 V and I_D = 200 mA (V_{GS} = -2.63 V) has been chosen. The quiescent current I_D corresponds approximately to 10 % of the maximum value (deep class AB), and it has been selected to fulfill the conditions for harmonic manipulation technique application [23].

Because the device may show negative impedance and potential oscillation issues at any working frequency, a stability network has been designed and ultimately placed between the HEMT gate and the input matching network.

Consequently, the scheme reported in Fig. 2(a) has been adopted, where the shunt R_P resistor and the series parallel L_S-C_S network guarantee low-frequency and in-band stability conditions, respectively. Fig. 2(b) shows the layout of the chosen stability network, where the inductor L_P has been realized through a shorted transmission line with 0.8 mm width (characteristic impedance Z_C = 23.3 Ω), which is compatible with the 0603 SMD package used for the other passive components (resistors and capacitors).

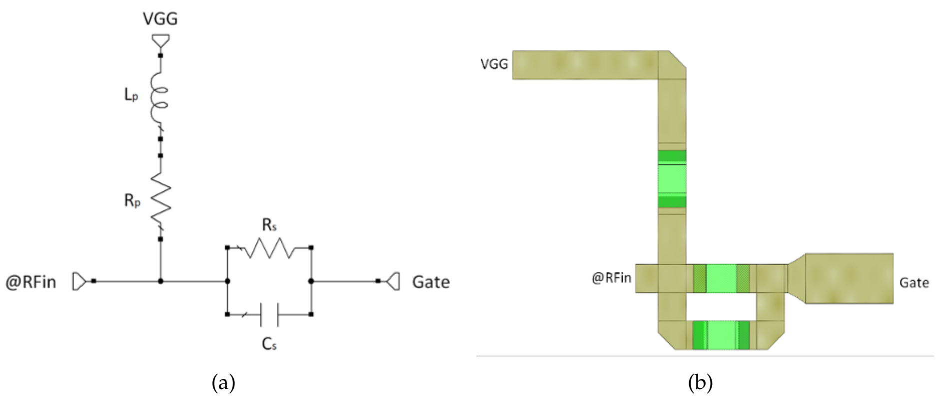

Figure 2. Stability network scheme (a) and layout realization (b).

From a theoretical point of view, the unconditional stability analysis of two-port microwave circuits may be performed in several ways, namely by the Rollet stability factor K and the scattering matrix determinant Δ [24,25], or by the geometric stability factors μ [26] or by the Nyquist criterion [27].

Fig. 3 shows that a geometric stability factor greater than 1 between 0 and 14 GHz has been achieved (R_P = 17 Ω, R_S = 6.8 Ω, C_S = 6.12 pF). In the same figure, $\mu \approx 2$ and a transducer gain (GMax) value of about 18 dB are outlined in the 3.0 – 4.0 GHz band, whereas the maximum available gain GMax, with and without the stability network, is reported as well.

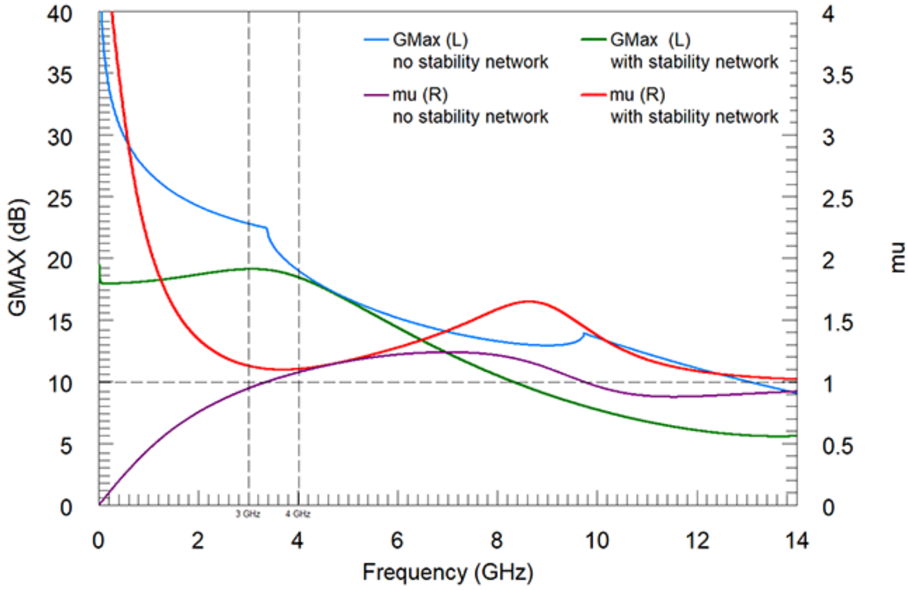

Figure 3. Effect of the stability network on maximum available gain (GMax) and geometric stability factor (mu).

3.3. Input & Output Matching Network

Optimum load (Γ_{out}) and source (Γ_{in}) impedances at the fundamental frequency have been found using source and load pull simulations. In this regard, load pull simulations are presented in Fig. 4, where Pout and PAE contours at 3.4 GHz, 3.55 GHz and 3.7 GHz, respectively, are outlined.

Next, ideal optimum input and output reflection coefficients (Γ_{in} and Γ_{out}) at the fundamental frequency of 3.55 GHz are reported, both in values (Table 1) and in graphical form (Fig. 5), whereas terminations up to the third harmonic have been defined using ideal tuners to maximize Pout, Gain and PAE of the whole amplifier.

It is worth to be noted that the optimum load is complex at the fundamental frequency of 3.55 GHz, since the output matching network has to transform the 50 Ω output load into complex impedance, whereas the optimal loads are purely reactive at harmonic frequencies.

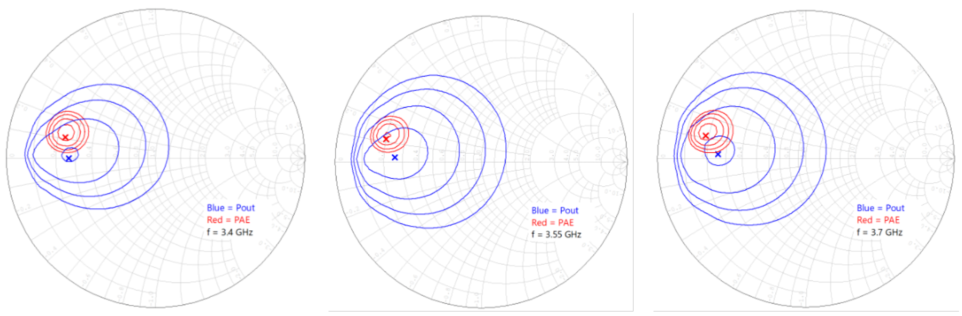

(a) (b) (c)

Figure 4. Load pull simulations at 3.4 GHz (a), 3.55 GHz (b) and 3.7 GHz (c).

In order to synthesize the above defined optimum load values for the multi harmonic tuned PA, the impedance transforming properties of transmission lines have been used to implement input and ouput matching networks. In fact, the reactive matching

Table 1. Optimum input and output harmonic load values.

Freq. (GHz)	Γ_{in} Ideal	Γ_{in} Synthesized	Γ_{out} Ideal	Γ_{out} Synthesized
3.7	$0.933\, e^{j\cdot 158^\circ}$	$0.933\, e^{j\cdot 157.6^\circ}$	$0.664\, e^{j\cdot 173^\circ}$	$0.664\, e^{j\cdot 172.8^\circ}$
7.4	$1\, e^{j\cdot 110^\circ}$	$0.980\, e^{j\cdot 108.2^\circ}$	$1\, e^{j\cdot 172^\circ}$	$0.994\, e^{-j\cdot 169.7^\circ}$
11.1	$1\, e^{j\cdot 38^\circ}$	$0.945\, e^{j\cdot 37.15^\circ}$	$1\, e^{j\cdot 141^\circ}$	$0.962\, e^{j\cdot 137.6^\circ}$

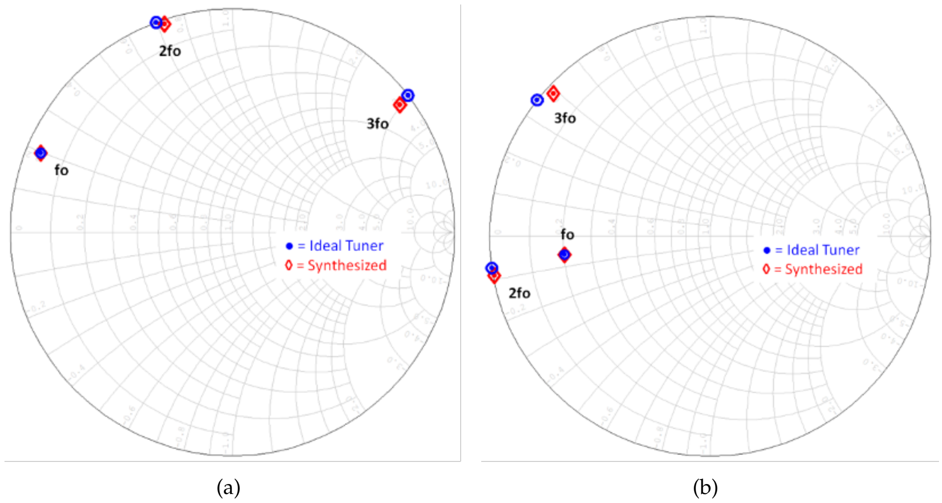

Figure 5. Optimum input (a) and output (b) harmonic loads, set them up with ideal tuners (circle symbols) and currently synthesized (diamond symbols).

method (single stub tuning) [28] has been used to design a reactive matching network for each harmonic.

According to this method, a series microstrip transmission line together with an open-circuited shunt stub can transform a 50-ohm, or any arbitrary load impedance, into the desired value of impedance. A general matching circuit schematic has been represented in Fig. 6, where $y_L = 1$ is the load normalized admittance ($Y_L = 1/50$ Siemens), $y_1 = \pm j \cdot b_1$ is the normalized admittance of the shunt open stub ($b_1 > 0$ for capacitive susceptance, $b_1 < 0$ for inductive susceptance, b_s always positive), and the length L_1 determines the value of $\pm j \cdot b_1$. The addition of $y_1 = \pm j \cdot b_1$ to y_L produces a motion along the unity constant-conductance circle from $y_L = 1$ to $y_2 = 1 \pm j \cdot b_1$. The series transmission line of length L_2 transforms y_2 into the desired normalized admittance y_{IN}. As a consequence, the value of b_1 must be selected so that y_2 and y_{IN} are on a constant $|\Gamma|$ circle.

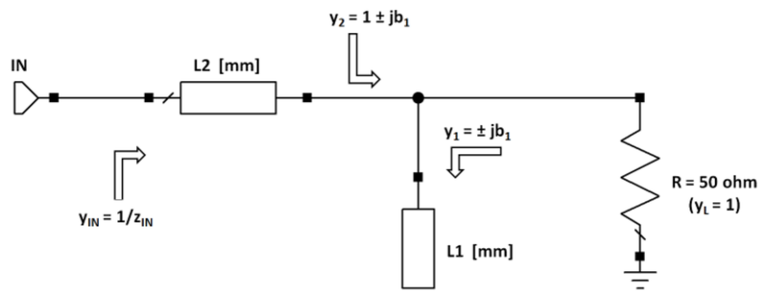

Figure 6. Reactive matching scheme.

The designed output matching network is presented in Fig. 7(a), where the transmission line and open stub matching network that controls each harmonic has been outlined (f_0 = 3.55 GHz). A constant microstrip width of 0.8 mm has been adopted (Z_C = 23.3Ω).

At first, the network has been designed with ideal transmission lines for each single frequency, then real microstrip elements have been introduced together with parasitic elements. Finally, the three matching networks have been assembled all together and the transmission line parameters have been optimized in order to achieve the desired impedance values.

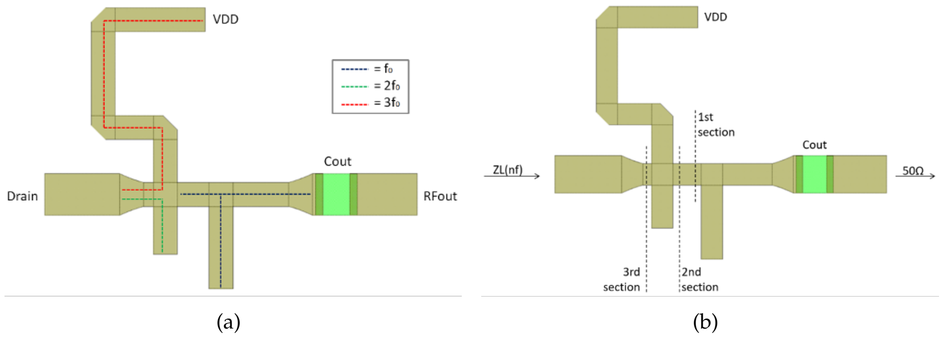

Figure 7. Output matching network: transmission line and open stub controlling each harmonic (a) and section planes used to synthesized the whole structure (b).

Furthermore, the output matching network has been synthesized using a three-section structure, as shown in Fig. 7(b), where the synthesized load at the matched port ($Z_L(nf)$) and the loads presented across each section are reported in Fig. 8 for the fundamental frequency (8(a)) and the second (8(b)) and third (8(c)) harmonic, in a larger frequency range from 3.3 to 3.8 GHz. Section planes are placed in such a way that they properly explore how the correspondent synthesized load changes its value, according to the above described reactive matching method.

The synthesized input matching network is depicted in Fig. 9(a), where the fundamental harmonic (f_0=3.55 GHz) has been controlled by a transmission line and an open stub, while another network has been designed and implemented for the control of both second and third harmonic simultaneously (the width of the 2^{nd} and 3^{rd} harmonic open stub is 0.24 mm, Z_C = 46.3 Ω). Such choice has led to a significant reduction of the amplifier dimensions.

Likewise the output matching network, the input matching network has been tested through three theoretical cutting in the whole structure, as shown in Fig. 9(b), whereas the actual loads at the matched port ($Z_S(nf)$) and across each section are reported in Fig. 10 for the fundamental frequency (10(a)) and the second (10(b)) and third (10(c)) harmonic as well, in the frequency range from 3.3 to 3.8 GHz.

Two capacitors acting as DC and low frequency signals block (C_{out}= 10 pF and C_{in}= 0.6 pF in Fig. 7 and Fig. 9, respectively), have been inserted into the matching networks.

Note that, in order to avoid electromagnetic coupling (cross-talk), the distance between two adjacent transmission lines was maintained always higher than $3 \cdot H \approx$0.8 mm, where H=0.254 mm is the substrate thickness.

The synthesized input and output reflection coefficients (Γ_{in} and Γ_{out}) are reported in the aforementioned Table 1 (value form) and Fig. 5 (graphical form, red diamond symbol), where the comparison with the correspondent ideal loads shows a very good agreement.

The input-output matching networks have also been electromagnetically simulated with the MoM (Method of Moment) electromagnetic simulator AXIEM, available inside the AWR-MWO software. Electromagnetic simulations can evidence some parasitic or coupling mechanisms, which are not taken into account by the AWR circuit model components. However, no significant variations have been evidenced.

The layout of the power amplifier is reported in Fig. 11. Dimensions of the whole amplifier (46 mm x 14 mm – LxH), stability network (10.7 mm x 8.4 mm – LxH), output

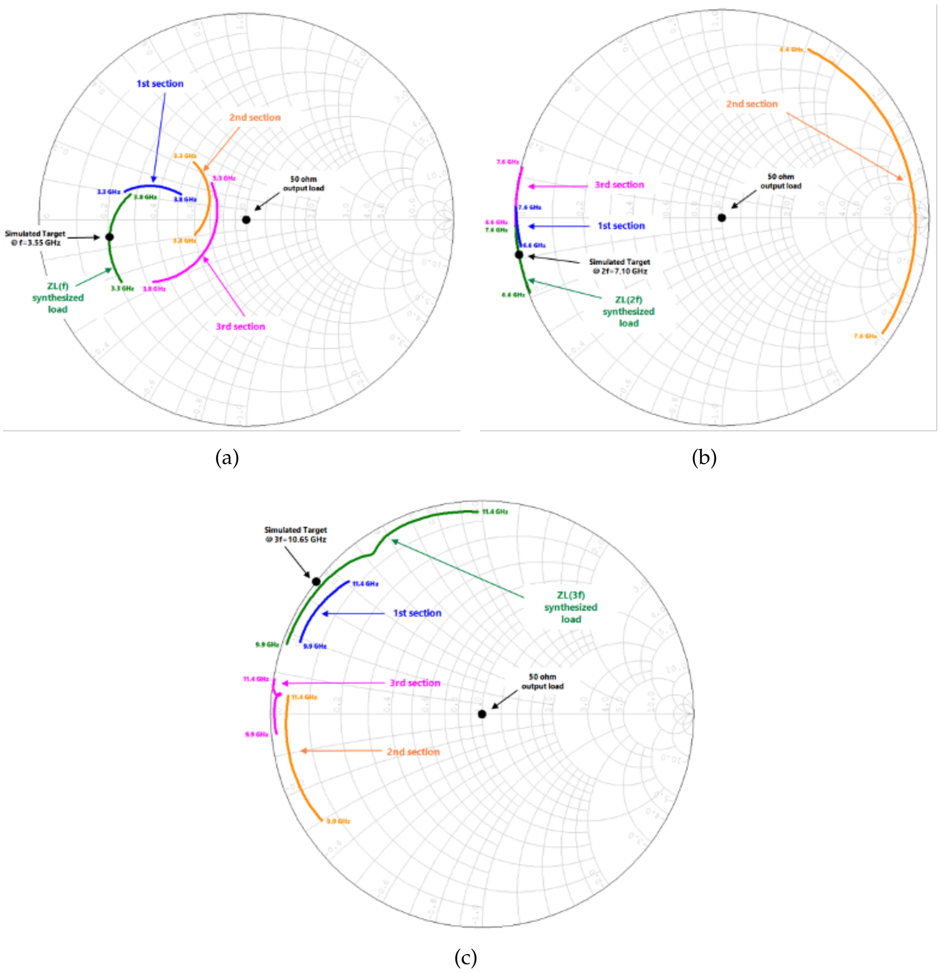

Figure 8. Output matching network: synthesized load at the matched port and across each matching network section, for the fundamental frequency (a), the second harmonic (b) and the third harmonic (c), in the frequency range from 3.3 to 3.8 GHz.

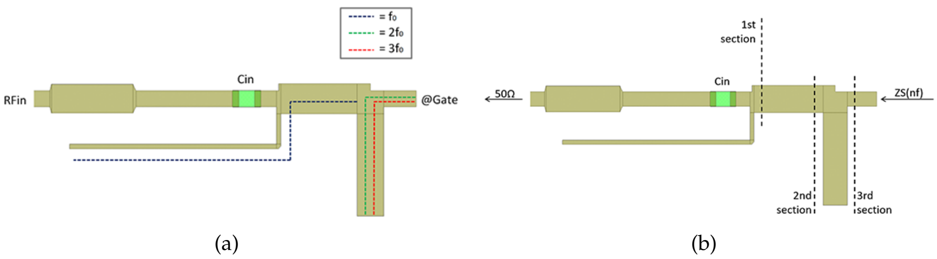

Figure 9. Input matching network: transmission line and open stub controlling each harmonic (a) and section planes used to synthesized the whole structure (b).

matching network (12.4 mm x 9.4 mm – LxH) and input matching network (22 mm x 6.5 mm – LxH) are reported.

Two biasing networks close to V_{GG} and V_{DD} pads made by capacitors and resistances, have been implemented in the final layout, to short circuit the RF signal and to reduce the eventual ripple in the bias voltages The presence of resistance components in the biasing network ensures a lower quality factor Q of the potential resonance effects, thus leading to an out-of-band $S_{11}(f)$ distribution gathered nearby the short circuit point in the Smith chart.

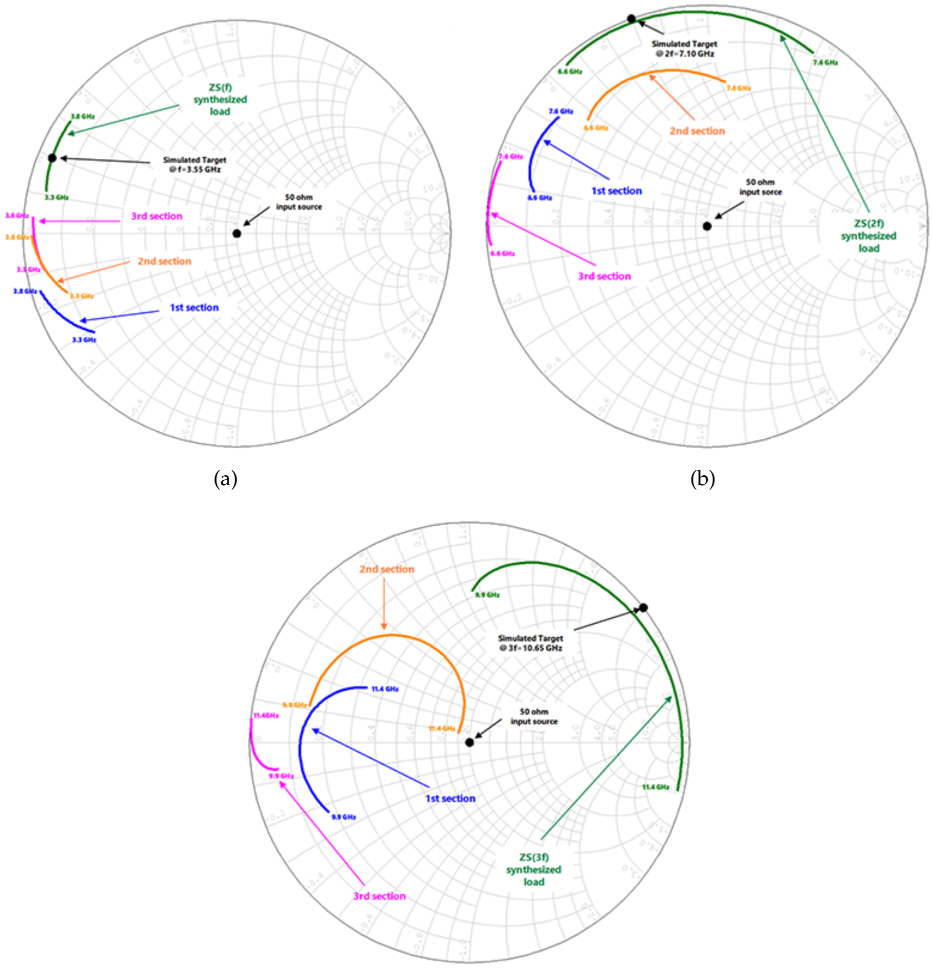

(a) (b)

(c)

Figure 10. Output matching network: synthesized load at the matched port and across each matching network section, for the fundamental frequency (a), the second harmonic (b) and the third harmonic (c), in the frequency range from 3.3 to 3.8 GHz.

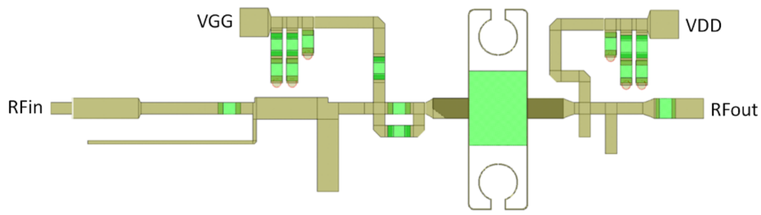

Figure 11. PA layout.

The intrinsic load curve (i.e., achieved across the intrinsic current source of the non linear HEMT model) at 1 dB compression point alongside with the static bias point overlapped to the extrinsic output characteristics are reported in Fig. 12. It was demonstrated in,[3] that the presence of the upper bending in the dynamic load line of a GaN HEMT, generates an output current waveform with a negative second harmonic current component. As a consequence, the fundamental and second harmonic currents are opposite in phase. This phase relation is mandatory, otherwise the use of an output second-harmonic termination becomes deleterious [19].

The fabricated PA is shown in Fig. 13, where two SMA connectors have been used to connect the amplifier to the RF source and the load. The resulting parasitic effects

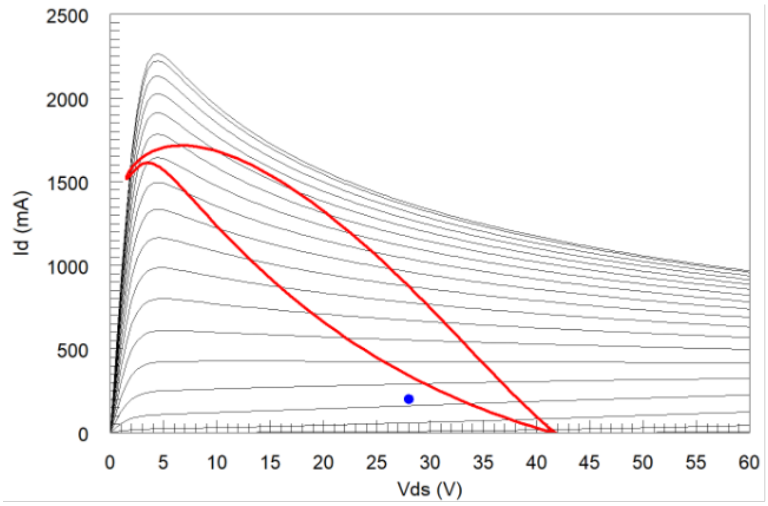

Figure 12. Simulated intrinsic load curve at 1 dBcp.

have been taken into account as well. At the same time, a Montecarlo analysis of the PA components has been performed, in order to maximize the performance of the whole power amplifier.

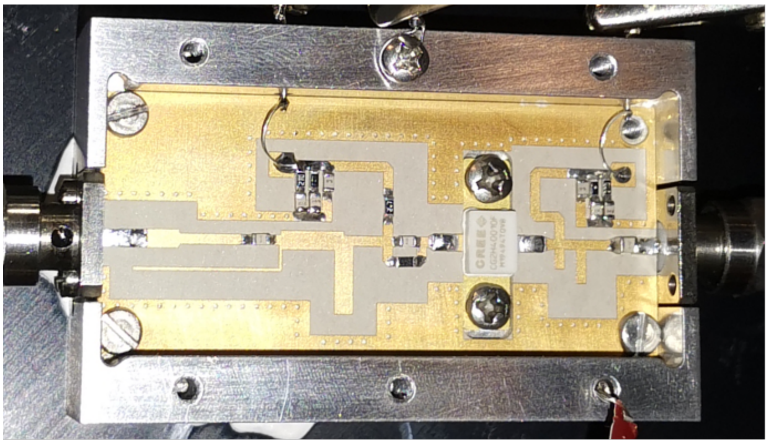

Figure 13. Photo of the realized PA.

4. Experimental Results

As already pointed out in section 3.1, GaN technology shows high power density. This leads to high dissipated power levels in a limited chip area, which makes the device heating a critical issue that needs to be taken into account. To sort this issue out, a proper heat sink with thermal paste as interface was placed below the PA device during the power measurements, as shown in Fig. 14.

The realized PA has been characterized both by linear and non-linear measurements. To define small-signal behavior, PA scattering parameters have been measured with a vector network analyzer.

Fig. 15 shows the measured scattering parameters of the PA evaluated at the bias point (V_{DS} = 28 V, I_D = 200 mA), together with the simulated ones. The substrate dielectric constant has been fixed to 11.2. A good agreement between simulation and measurements have been reported, particularly on S_{21} magnitude in the working frequency band 3.4 GHz - 3.7 GHz.

To define large signal behavior in a continuous wave mode, PA parameters have been measured using a LabView controlled measurement system available at MECSA

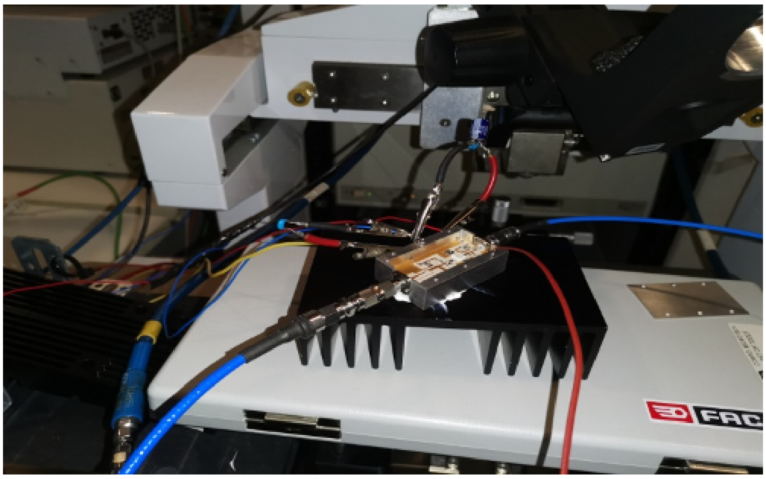

Figure 14. Photo of the power amplifier under measurements.

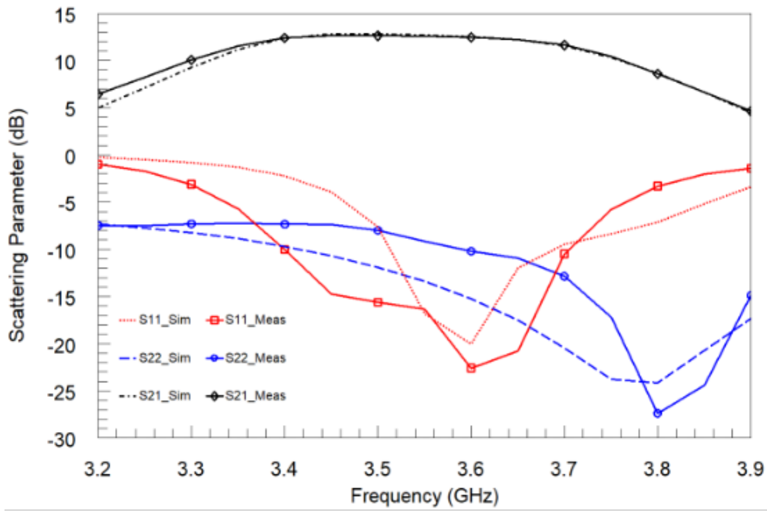

Figure 15. PA linear performance.

Tor Vergata University of Rome Labs. The system is based on a Signal generator and on a Agilent E4448A spectrum analyzer.

Measured PA data at 3.4 GHz, 3.55 GHz, 3.7 GHz for the nominal bias condition (I_D = 200 mA, V_{DS} = 28 V) and the comparison with simulated results (after reverse engineering models update) are reported in Fig. 16), respectively. Moreover, measured PAE in the frequency range 3.2 GHz - 3.8 GHz are depicted in Fig. 17. A saturated output power Pout = 42.27 dBm with power gain GP = 9.3 dB and PAE = 53.5 % (drain efficiency = 60 %), were obtained at 3.7 GHz.

Next, the PA has been characterized in the frequency range from 3.2 to 3.9 GHz, with a 33 dBm of fixed input available power, corresponding to the PAE peak. Results are reported in Fig. 18 and compared with simulated counterparts. The achieved results show a ripple in the output power and power gain lower than 1 dB, and a PAE value higher than 45 %, in the frequency range 3.3 GHz - 3.8 GHz.

Comparisons of this PA performance with the state of the art of S band GaN PAs are reported in Table 2 (and showed in graphical form in Fig. 19.

5. Conclusions

In this paper, the design and the physical realization of an S band multi harmonic tuned power amplifier in GaN technology and hybrid form have been presented. The amplifier's small and large signal performance have been shown and discussed. In an operating bandwidth of 300 MHz around f_0=3.55 GHz (8.4 % of fractional bandwidth),

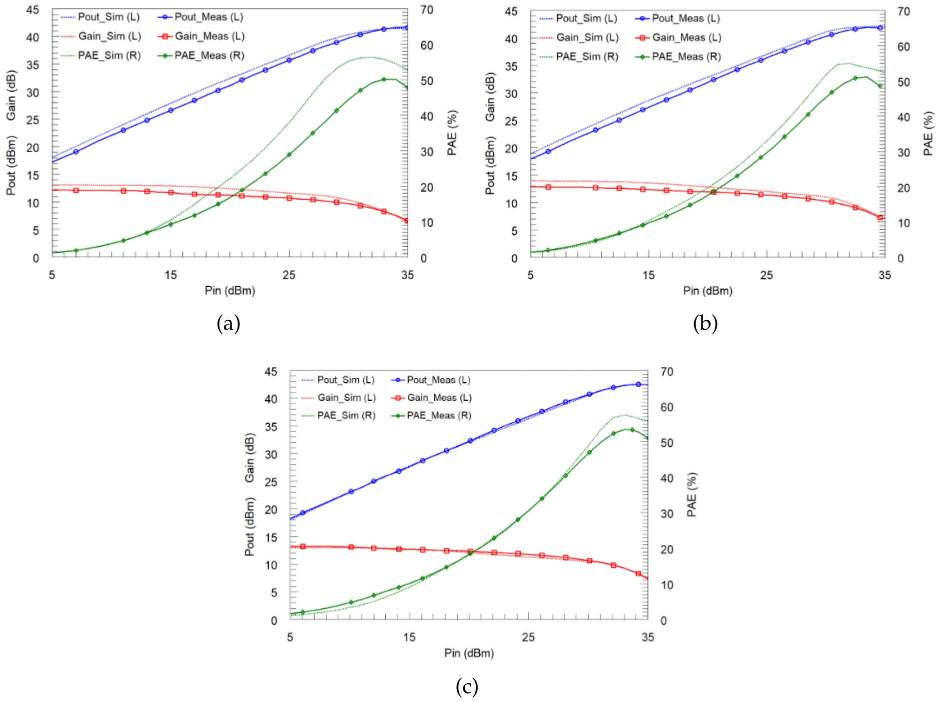

Figure 16. Power amplifier performance at 3.4 GHz (a), 3.55 GHz (b) and 3.7 GHz (c).

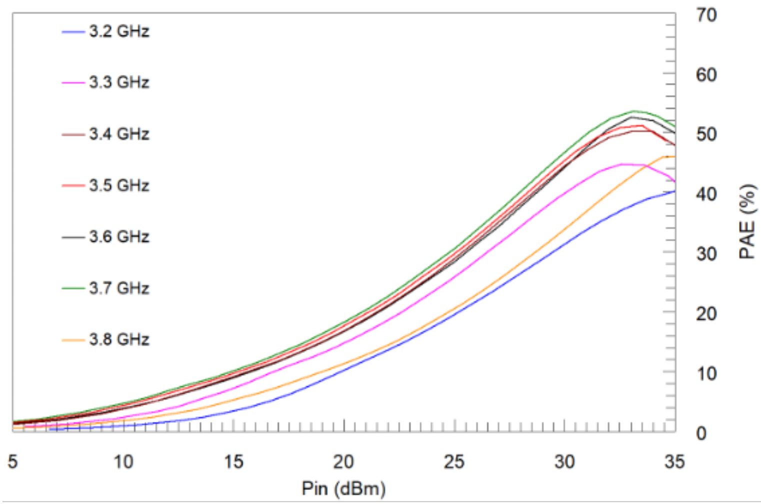

Figure 17. Measured PAE values in the frequency range 3.2 GHz - 3.8 GHz.

experimental results demonstrate 42.3 dBm output power, 9.3 dB power gain and 53.5 % PAE (60 % drain efficiency) at 3.7 GHz.

Author Contributions: Conceptualization, S.G..; writing—original draft preparation, S.G. and S.P.; writing—review and editing, S.G. and P.C..; supervision, P.C. All authors have read and agreed to the published version of the manuscript.

Funding: This research received no external funding

Conflicts of Interest: The authors declare no conflict of interest.

Abbreviations

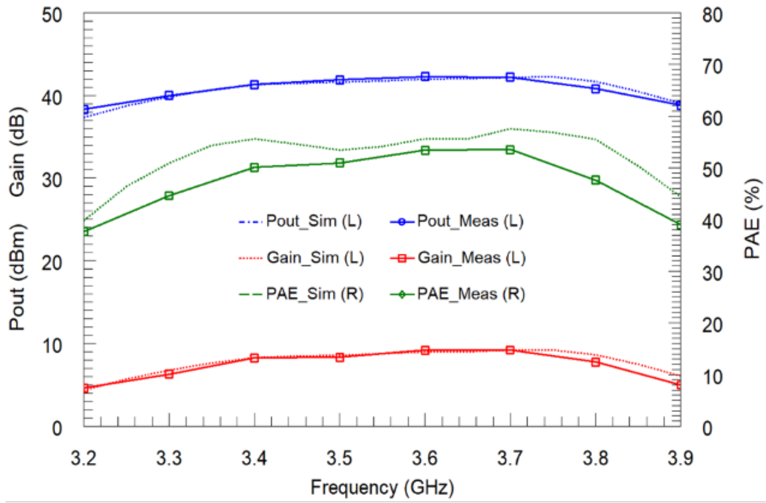

Figure 18. PA performance at Pin = 33 dBm.

Table 2. State of the art of GaN PA's.

Ref.	Year	Freq (GHz)	Pout (dBm)	PAE (%)	Gain (dB)
[9]	2017	3.7	40.7	46.8	10
[29]	2017	3.5	40	48	10.5
[30]	2018	3.5	41.7	47.5	9
[31]	2019	3.5	43.4	52.6	14
[32]	2020	3.7	38	61	10
[33]	2020	3.6	38.5	52	12.8
[34]	2021	3.6	39.9	52	7.2
T.W.	**2021**	**3.7**	**42.3**	**53.5**	**9.3**

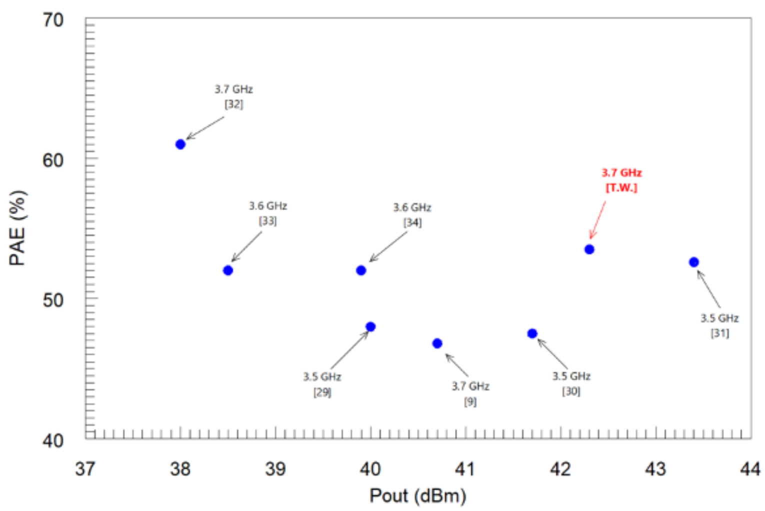

Figure 19. State of the art of GaN PA's in graphical form.

300 The following abbreviations are used in this manuscript:

EM	Electromagnetic
PA	power Amplifier
GaN	Gallium Nitride
IMN	Input Matching Network
OMN	Output Matching Network

References

1. Raab, F.; Asbeck, P.; Cripps, S.; Kenington, P.; Popovic, Z.; Pothecary, N.; Sevic, J.; Sokal, N. Power amplifiers and transmitters for RF and microwave. *IEEE Transactions on Microwave Theory and Techniques* **2002**, *50*, 814–826. doi:10.1109/22.989965.
2. Prejs, A.; Wood, S.; Pengelly, R.; Pribble, W. Thermal analysis and its application to high power GaN HEMT amplifiers. 2009 IEEE MTT-S International Microwave Symposium Digest, 2009, pp. 917–920. doi:10.1109/MWSYM.2009.5165847.
3. Colantonio, P.; Limiti, E.; Giannini, F. *High efficiency RF and microwave solid state power amplifiers*; Wiley series in microwave and optical engineering, Wiley: Chichester, U.K, 2009.
4. Raab, F. Maximum efficiency and output of class-F power amplifiers. *IEEE Transactions on Microwave Theory and Techniques* **2001**, *49*, 1162–1166. doi:10.1109/22.925511.
5. Colantonio, P.; Giannini, F.; Leuzzi, G.; Limiti, E. On the class-F power amplifier design. *International Journal of RF and Microwave Computer-Aided Engineering* **1999**, *9*, 129–149. doi:https://doi.org/10.1002/(SICI)1099-047X(199903)9:2<129::AID-MMCE7>3.0.CO;2-U.
6. Raab, F. Class-F power amplifiers with maximally flat waveforms. *IEEE Transactions on Microwave Theory and Techniques* **1997**, *45*, 2007–2012. doi:10.1109/22.644215.
7. Raffo, A.; Vadalà, V.; Bosi, G.; Trevisan, F.; Avolio, G.; Vannini, G. Waveform engineering: State-of-the-art and future trends (invited paper). *International Journal of RF and Microwave Computer-Aided Engineering* **2017**, *27*, e21051. doi:https://doi.org/10.1002/mmce.21051.
8. Liu, G.; Li, S.; Cheng, Z.; Feng, H.; Dong, Z. High-efficiency broadband GaN HEMT power amplifier based on harmonic-tuned matching approach. *International Journal of RF and Microwave Computer-Aided Engineering* **2020**, *30*, e22097. doi:https://doi.org/10.1002/mmce.22097.
9. Olavsbråten, M.; Mathiesen, T.; Berry, E. Design of an efficient wideband (1–5GHz) 10W PA in GaN technology using harmonic tuning. 2017 IEEE 18th Wireless and Microwave Technology Conference (WAMICON), 2017, pp. 1–5. doi:10.1109/WAMICON.2017.7930267.
10. Colantonio, P.; Giannini, F.; Giofre, R.; Limiti, E.; Serino, A.; Peroni, M.; Romanini, P.; Proietti, C. A C-band high-efficiency second-harmonic-tuned hybrid power amplifier in GaN technology. *IEEE Transactions on Microwave Theory and Techniques* **2006**, *54*, 2713–2722. doi:10.1109/TMTT.2006.874872.
11. Li, S.; Lin, V.C.; Nandhasri, K.; Ngarmnil, J. New high-efficiency 2.5 V/0.45 W RWDM class-D audio amplifier for portable consumer electronics. *IEEE Transactions on Circuits and Systems I: Regular Papers* **2005**, *52*, 1767–1774. doi:10.1109/TCSI.2005.852500.
12. Dooley, J.; Farrell, R. A Practical Class S Power Amplifier for High Frequency Transmitters. Royal Irish Academy Colloquium on Emerging Trends in Wireless Communications 2008, 2008.
13. Sokal, N. Class E high-efficiency power amplifiers, from HF to microwave. 1998 IEEE MTT-S International Microwave Symposium Digest (Cat. No.98CH36192), 1998, Vol. 2, pp. 1109–1112 vol.2. doi:10.1109/MWSYM.1998.705187.
14. Smith, R.; Glynn, S.; Greene, J.; Devlin, L. A Fully Integrated 3.5GHz Single Chip GaN Doherty PA for sub-6GHz 5Ge. https://www.rfglobalnet.com/doc/a-fully-integrated-ghz-single-chip-gan-doherty-pa-for-sub-ghz-g-0001, 2019. [Online; accessed 4-July-2021].
15. G.S.A, G.M.S.A. Spectrum for Terrestrial 5G Networks: Licensing Developments Worldwide. http://comitatomcs.eu/wp-content/uploads/2019/08/190730-GSA-5G-spectrum-report-July.pdf, 2019. [Online; accessed 22-July-2021].
16. Barret, J.G.M.S.A.G. 5G Spectrum bands. https://gsacom.com/5g-spectrum-bands/, 2017. [Online; accessed 22-July-2021].
17. Abbasian, S.; Johnson, T. Effect of Second and Third Harmonic Input Impedances in a Class-F Amplifier. *Progress In Electromagnetics Research C* **2015**, *56*, 39–53. doi:10.2528/PIERC14101410.
18. Li, X.; Colantonio, P.; Giannini, F.; Yu, H.; Lin, C. S-Band Class-C-F Power Amplifier with 2nd Harmonic Control at the Input. *Applied Sciences* **2020**, *10*. doi:10.3390/app10010259.
19. Colantonio, P.; Giannini, F.; Leuzzi, G.; Limiti, E. Multiharmonic manipulation for highly efficient microwave power amplifiers. *International Journal of RF and Microwave Computer-Aided Engineering* **2001**, *11*, 366–384. doi:https://doi.org/10.1002/mmce.1045.
20. Colantonio, P.; Giannini, F.; Leuzzi, G.; Limiti, E. Very high efficiency microwave amplifier. The harmonic manipulation approach. 13th International Conference on Microwaves, Radar and Wireless Communications. MIKON - 2000. Conference Proceedings (IEEE Cat. No.00EX428), 2000, Vol. 3, pp. 33–46 vol.3. doi:10.1109/MIKON.2000.914042.
21. Pengelly, R.S.; Wood, S.M.; Milligan, J.W.; Sheppard, S.T.; Pribble, W.L. A Review of GaN on SiC High Electron-Mobility Power Transistors and MMICs. *IEEE Transactions on Microwave Theory and Techniques* **2012**, *60*, 1764–1783. doi:10.1109/TMTT.2012.2187535.
22. Pisa, S.; Chicarella, S.; Cusani, R.; Citrolo, J. 30–512 MHz power amplifier design using GaN transistor. *Microwave and Optical Technology Letters* **2018**, *60*, 1280–1286. doi:https://doi.org/10.1002/mop.31155.
23. Colantonio, P.; Giannini, F.; Leuzzi, G.; Limiti, E. Theoretical facet and experimental results of harmonic tuned PAs. *International Journal of RF and Microwave Computer-Aided Engineering* **2003**, *13*, 459–472. doi:https://doi.org/10.1002/mmce.10106.
24. Rollett, J. Stability and Power-Gain Invariants of Linear Twoports. *IRE Transactions on Circuit Theory* **1962**, *9*, 29–32. doi:10.1109/TCT.1962.1086854.
25. Woods, D. Reappraisal of the unconditional stability criteria for active 2-port networks in terms of S parameters. *IEEE Transactions on Circuits and Systems* **1976**, *23*, 73–81. doi:10.1109/TCS.1976.1084179.

26. Edwards, M.; Sinsky, J. A new criterion for linear 2-port stability using a single geometrically derived parameter. *IEEE Transactions on Microwave Theory and Techniques* **1992**, *40*, 2303–2311. doi:10.1109/22.179894.
27. Pisa, S.; Zolesi, M. A method for stability analysis of small-signal microwave amplifiers. *International Journal of RF and Microwave Computer-Aided Engineering* **1998**, *8*, 293–302. doi:https://doi.org/10.1002/(SICI)1099-047X(199807)8:4<293::AID-MMCE3>3.0.CO;2-H.
28. Gonzalez, G. *Microwave Transistor Amplifiers (2nd Ed.): Analysis and Design*; Prentice-Hall, Inc.: USA, 1996.
29. Drews, S.; Rautschke, F.; Maassen, D.; Nghe, C.T.; Boeck, G. A 10-W S-band power amplifier for future 5G communication. 2017 47th European Microwave Conference (EuMC), 2017, pp. 152–155. doi:10.23919/EuMC.2017.8230822.
30. Duffy, M.R.; Berry, E.; Lasser, G.; Popović, Z. An Efficient Linearized Octave-Bandwidth Power Amplifier for Carrier Aggregation. 2018 IEEE/MTT-S International Microwave Symposium - IMS, 2018, pp. 473–476. doi:10.1109/MWSYM.2018.8439701.
31. Smith, R.; Devlin, L.; Tran, K.; Martin, R. An Adaptable GaN Power Amplifier for S-Band Radar. https://www.prfi.com/wp-content/uploads/2019/10/An-Adaptable-GaN-Power-Amplifier-for-S-Band-Radar.pdf, 2021. [Online; accessed 22-July-2021].
32. Liu, C.; Li, X.; Zhao, Y.; Qi, T.; Du, X.; Chen, W.; Ghannouchi, F.M. Investigation of High-Efficiency Parallel-Circuit Class-EF Power Amplifiers With Arbitrary Duty Cycles. *IEEE Transactions on Industrial Electronics* **2021**, *68*, 5000–5012. doi:10.1109/TIE.2020.2991924.
33. Zhou, L.H.; Zhou, X.Y.; Chan, W.S.; Sharma, T.; Ho, D. Wideband Class-F-1 Power Amplifier With Dual-Quad-Mode Bandpass Response. *IEEE Transactions on Circuits and Systems I: Regular Papers* **2020**, *67*, 2239–2249. doi:10.1109/TCSI.2020.2978914.
34. Ochoa-Armas, D.; Lavandera-Hernández, I.; Fernández-Ramón, D.; Loo-Yau, J.R.; Molina-Ceseña, M.; Pérez-Wences, C.; Hernández-Domínguez, E.A.; Reynoso-Hernández, J.A.; Moreno, P. A nonlinear empirical I/V model for GaAs and GaN FETs suitable to design power amplifiers. *International Journal of RF and Microwave Computer-Aided Engineering* **2021**, *31*, e22552. doi:https://doi.org/10.1002/mmce.22552.